

Comparative investigation of microjetting generated from monocrystalline tin surface and polycrystalline tin surface under plane impact loading

Shao-Wei Sun(孙少伟), Guan-Qing Tang(汤观晴), Ya-Fei Huang(黄亚飞), Liang-Zhi Cao(曹良志), and Xiao-Ping Ouyang(欧阳晓平)

Citation: Chin. Phys. B, 2021, 30 (**10**): 104701. DOI: 10.1088/1674-1056/abeeea
Journal homepage: http://cpb.iphy.ac.cn; http://iopscience.iop.org/cpb

What follows is a list of articles you may be interested in

Energy stored in nanoscale water capillary bridges formed between chemically heterogeneous surfaces with circular patches

Bin-Ze Tang(唐宾泽), Xue-Jia Yu(余雪佳), Sergey V. Buldyrev, Nicolas Giovambattista§, and Li-Mei Xu(徐莉梅)¶
Chin. Phys. B, 2020, 29 (**11**): 114703. DOI: 10.1088/1674-1056/abb664

Molecular-dynamics investigation of the simple droplet critical wetting behavior at a stripe pillar edge defect

Xiaolong Liu(刘小龙), Chengyun Hong(洪成允), Yong Ding(丁勇), Xuepeng Liu(刘雪朋), Jianxi Yao(姚建曦), Songyuan Dai(戴松元)
Chin. Phys. B, 2019, 28 (**1**): 014703. DOI: 10.1088/1674-1056/28/1/014703

Numerical simulations of dense granular flow in a two-dimensional channel:The role of exit position

Tingwei Wang(王廷伟), Xin Li(李鑫), Qianqian Wu(武倩倩), Tengfei Jiao(矫滕菲), Xingyi Liu(刘行易), Min Sun(孙敏), Fenglan Hu(胡凤兰), Decai Huang(黄德财)
Chin. Phys. B, 2018, 27 (**12**): 124704. DOI: 10.1088/1674-1056/27/12/124704

Theoretical studies and molecular dynamics simulations on ion transport properties in nanochannels and nanopores

Ke Xiao(肖克), Dian-Jie Li(李典杰), Chen-Xu Wu(吴晨旭)
Chin. Phys. B, 2018, 27 (**2**): 024702. DOI: 10.1088/1674-1056/27/2/024702

Nano watermill driven by revolving charge

Zhou Xiao-Yan, Kou Jian-Long, Nie Xue-Chuan, Wu Feng-Min, Liu Yang, Lu Hang-Jun
Chin. Phys. B, 2015, 24 (**7**): 074702. DOI: 10.1088/1674-1056/24/7/074702

Comparative investigation of microjetting generated from monocrystalline tin surface and polycrystalline tin surface under plane impact loading

Shao-Wei Sun(孙少伟)[1,3], Guan-Qing Tang(汤观晴)[2,3], Ya-Fei Huang(黄亚飞)[3], Liang-Zhi Cao(曹良志)[1,†], and Xiao-Ping Ouyang(欧阳晓平)[1,‡]

[1] *School of Energy and Power Engineering, Xi'an Jiaotong University, Xi'an* 710049, *China*
[2] *College of Materials Science and Engineering, Hunan University, Changsha* 410082, *China*
[3] *Institute of Fluid Physics, China Academy of Engineering Physics, Mianyang* 621999, *China*

(Received 11 January 2021; revised manuscript received 1 March 2021; accepted manuscript online 16 March 2021)

With considering the scattering effect of grain boundary and the grain orientation, the molecular dynamics is used for the first time to comparatively investigate microjetting generated by monocrystalline tin surface and polycrystalline tin surface under plane impact loading in this work. The research results show that when the impact velocity is low, the scattering effect of grain boundary and different grain orientations in a polycrystalline tin will cause the sample to melt inhomogeneously, leading the shock wave front to attenuate, meanwhile, the inhomogeneous melting can result in jet deviating. Comparing with monocrystalline tin, the jet head velocity, jet velocity coefficient, and jet mass coefficient of polycrystalline tin at low impact velocity are all low. Moreover, as the impact velocity increases, this influence decreases and the microjetting results of polycrystalline tin and monocrystalline tin tend to be consistent with each other.

Keywords: molecular dynamics, shock wave, microjetting, monocrystalline tin, polycrystalline tin

PACS: 47.11.Mn, 47.40.Nm, 31.15.xv, 34.20.Cf **DOI:** 10.1088/1674-1056/abeeea

1. Introduction

When the compression shock wave is reflected from the free surface of a material, the surface of the material can be broken due to the complex interaction between the shock wave and surface defects.[1] The microscopic jet can be ejected from the surface, forming micron-sized particle fragments, which is called the microjetting.[2] The microjetting occurs in front of the free surface of the impacted material, and it has been studied by the investigators of impact compression circle for decades. The microjetting can not only interfere with the diagnostics used to characterize the dynamics of materials (such as measuring the free surface velocity of materials), but also become a source of inhibiting applications such as in inertial confinement fusion.[3] Particularly, the microscopic jet produced by impacting metal materials is a substance that melts at a high speed and the research on this substance has broad application prospects in weapon design and equipment defense. Therefore, as an extremely important subject of current engineering application research, the investigation of microjetting has vital practical significance.

Previous experiments and theories focused mainly on the jet mass, the jet head velocity, the jet morphology, the molten state of the ejected substance, and other important factors.[4–7] The Los Alamos Laboratory used high-speed photography to find the differences between the jet volume and distribution of the microjetting material under the loading of unsupported shock waves and those under the loading of supported shock waves, and also measured the pressure ranges where the jet mass coefficient increased rapidly under the two loading methods.[8–10] de Rességuier *et al*. studied the microjetting characteristics of tin, aluminum, copper, and gold under laser shock loading and their results showed that the jet head velocity under laser shock loading is about 2–4 times the free surface velocity.[11] Chu *et al.* adopted the high-energy x-ray imaging technology to diagnose the microwire experiment of tin metal loaded by laser shock, and obtained the original image of the dynamic fragmentation of tin, and corrected its area density, bulk density and mass-velocity distribution.[12] Investigating the explosion and impact of tin with surface roughness of 10 in–250 in (1 in = 2.54 cm), Vogan *et al.* discovered that the jet mass changes significantly with the groove morphology and cannot be estimated by the defect mass alone.[13] Holtkamp *et al.* found that the surface fracture is caused by the continuous growth and connection of a large number of micro-holes after melting through adopting the proton photography to study the material morphology of the microjetting.[14] Although lots of research results have been obtained in experiment, the experimental results can only give images at a few specific moments, rather than the picture of the entire process. So, experiments are difficult to quantify the influences of these factors, which makes the effective information very

†Corresponding author. E-mail: caolz@mail.xjtu.edu.cn
‡Corresponding author. E-mail: oyxp2003@aliyun.com

© 2021 Chinese Physical Society and IOP Publishing Ltd

limited. Therefore, it is essential to use the numerical simulation. At present, the hydrodynamics simulation and molecular dynamics (MD) simulation are predominant.[6,7] Roland *et al.* used the smoothed particle hydrodynamics (SPH) to study the size distribution of fragments in copper samples loaded by laser shock, and at the same time quantified the effect of distance between particles and smooth length on the results.[15] Dyachkov *et al*. compared the results of the SPH simulation with the experimental results, showing that the size of the surface defects has a greater influence on the jet head velocity.[16] Soulard *et al*. investigated the surface failure characteristics of metallic copper under triangular wave loading by MD simulation, mainly analyzing the surface characteristics of impact melting and unloading melting, and calculated the curves required for thermodynamic analysis such as shock Hugoniot line and shock melting line.[17] Their results indicated that unloading melting make the material strength very small and negligible. Durand and Soulard discovered that the microjetting is stretched and decomposed to form particles of various sizes through MD simulation method.[18] They also simulated the static and dynamic fragmentation of the metallic tin liquid film formed in the later stage of the microjetting, which demonstrates that a thin layer of liquid metal produces more pores and smaller aggregates than a thick layer of liquid metal.[19] Combining the above brief review, we can see that the numerical simulation plays an indispensable role in studying the microjetting.

In summary, it is not difficult to find that both experimental investigations and numerical simulations have done quite sufficient and in-depth work on the microjetting research. Unfortunately, due to an ultra-fast process of the substance ejected from the defect under impact loading, it is hard to capture more available information through the current diagnostic methods experimentally. On the other hand, experimental design is difficult and easily interfered by many factors, which leads to difference in the accuracy of the results and a lack of systematic cognition and understanding of the microjetting. These barriers bring certain difficulties and challenges to the explaining of the related mechanism of the microjetting. With the further improvement of performance of computers, thereby greatly promoting the position of computational simulation in scientific research, the numerical simulation methods are urgently needed in the research of microjetting field. However, metal samples used in previous microjetting studies of numerical simulations are almost all monocrystalline, while most metals existing in nature are polycrystalline, and metal samples used in the experiments are almost all polycrystalline. The results of the numerical simulations should be regressed to the experiments and cannot be separated from the experimental results. Therefore, it is necessary to explore the microjetting phenomenon of impact loading monocrystalline metal and impact loading polycrystalline metal via numerical simulations.

Compared with monocrystalline metals, polycrystalline metals have complex grain orientations and a large number of grain boundaries among grains. In the early days, Meyers found that different grain orientations cause shock waves' velocities to be anisotropic, resulting in the increase of the width of the shock wave front.[20] Subsequently, Barber established a theoretical model to estimate the widths of the shock wave front of different metal materials.[21] Kadau *et al*.[22] compared the MD simulation results of impact loading monocrystalline iron with those of impact loading polycrystalline iron and revealed that the polycrystalline structure forms nuclei faster at the grain boundary than the monocrystalline structure. They claimed that the speed of the shock wave is affected by effects such as changes in grain orientation and grain boundary scattering, and that the width of the shock wave front increases with time, but the final shock Hugoniot function of monocrystalline and polycrystalline is convergent with the increase of particle speed.[22] Obviously, previous research results indicate that polycrystalline with the complex grain orientation and grain boundary scattering has a significant effect on the shock wave propagation process. However, shock wave is a key prerequisite factor for microjetting, with the numerical simulation methods applied to shock wave research, corresponding microjetting mechanisms need to be revealed on an atomic scale. In particular, the mechanism of the microjetting phenomenon of polycrystalline material with defects under impact loading needs to be further clarified. Therefore, this paper adopts the mainstream MD simulation method and selects tin commonly used in experiment to conduct a comparative study of the microjetting phenomenon of polycrystalline tin and that of monocrystalline tin under impact loading for the first time. In this paper, while considering the complex grain orientation and grain boundary scattering effects, the results of the jet head velocity, jet morphology, jet mass coefficient of monocrystalline tin and polycrystalline tin under the same impact loading are analyzed and discussed. This work will provide corresponding reference and new perspective for understanding the microjetting phenomenon and illustrating microjetting mechanism.

2. MD simulation

2.1. Theoretical background

The calculation principle of MD is to first construct a particle system with a large number of molecules or atoms. The motion law of atom and motion law of molecule in the system follow the Newton's second law of motion, namely,

$$F_i(t) = m_i a_i(t), \tag{1}$$

where force F can be derived from the position r by the potential energy E, and the velocity v and the position r can be obtained by the first and second integral of the acceleration a with respect to time t as follows:

$$m_i \frac{\partial_{vi}}{\partial_t} = F_i = -\frac{\partial E}{\partial_{ri}}, \tag{2}$$

$$\frac{\partial_{ri}}{\partial_t} = v(t). \tag{3}$$

The MD calculation is to solve the Newtonian equation of motion through the interaction potential, atomic coordinates and time step.[23,24] The initial structure is first constructed, that is, the initial coordinates of each atom in the entire system are arranged, and the force of each atom is determined by the interaction potential. According to the formula, the acceleration of each atom can be derived. The initial coordinates, initial velocity and acceleration of the atom at time zero are obtained by assigning the initial velocity of each atom at a certain temperature. By setting the time step Δt, the position and velocity of each atom can be obtained after time Δt. Through the continuous cycle of the above process, after reaching the target time t, all atomic positions and velocities in each interval of Δt can be obtained.[23,25] Moreover, the information about the basic properties of the material, the positions of dislocation, phase transformation, twin crystal, *etc*. can be obtained through statistical mechanics and structural analysis methods.[26] Therefore, compared with other simulation methods, MD simulation can provide some unique advantages. For example, it can directly simulate the formation, evolution and fragmentation process of microjetting based on the interaction potential between atoms, without inputting other physical models or parameters such as surface tension or viscosity. Owing to the unique ability of MD simulation to directly simulate dynamic fragments, which greatly meets the experimental research needs for precise physical cognition.[25,27] This is also the primary reason for choosing MD simulation in this article. What needs to be pointed out is that special attention should be paid when comparing MD results with experimental data, because the small size of the sample in MD may cause differences among the experimental results due to surface tension and other reasons, which requires further analysis.

In this paper, the MD simulations are performed with a large-scale atomic/molecular massively parallel simulator (LAMMPS).[28] In the polycrystalline model, it is necessary to build a sufficiently large model due to the existence of crystal grains, while the expansion of the model system in MD increases the amount of calculation exponentially. The EAM potential function in the calculation efficiency and the pertinence of tin properties is significantly higher than the MEAM and 2NN MEAM potential function considering the influence of the bond angle.[29–31] Therefore, the MD simulation study of the monocrystalline tin and polycrystalline tin with sinusoidal defects loaded on the plate is used by EAM potential function developed by Sapozhnikov.[32] This potential function is often used in the study of microjetting phenomena due to its close relationship with the experiment and the impact fusion line. In fact, EAM is originally proposed by Daw and Baskes.[33] The basic idea of EAM is that each atom in the system is assumed to be embedded in the electron cloud background generated by all other neighboring atoms. The interaction potential function between atoms is divided mainly into two parts: the first part is the interaction between atoms, and the second part is the embedding energy of the atom embedded in the electron cloud background. The EAM potential function is often used in numerical simulations related to various metal materials, and its expression is as follows:

$$E = \frac{1}{2}\sum_{i \neq j} \emptyset(r_{ij}) - \sum_i F(\rho_i), \tag{4}$$

where the first term on the right-hand side of the above formula is the interaction energy of the interaction between atoms, and the second term is the embedding energy of atoms embedded in the background electron cloud. The embedding energy can be expressed as a functional of charge density, and the relevant parameters in the two EMA potentials of tin are all listed in Table 1. This article will not repeat them here in detail, readers may refer to the relevant literature.[33]

Table 1. Parameters of two EAM potentials for tin interaction potential.

	$E^{(\mathrm{coh})}$ (eV)	A	n	Z	$r_{\max}$ (Å)	$r_{\min}$ (Å)	$\beta^{(0)}$	r (Å)
Set 1	1.8475	1.401	0.724	7.618	5.599	1.0	6	3.437
Set 2	1.8475	1.401	0.724	7.618	5.599	1.0	6	3.437
	E	α	D	η	μ			
Set 1	0.30625	3.314		2.41				
Set 2	0.32190	3.072	0.145	2.72	–1.87			

Since the studying object of this article is tin material, it is necessary to give a briefing of itin material. At present, the experimental research of microjetting focuses mainly on iron, aluminum, copper, lead, tin, *etc*. The low melting point characteristics of tin, lead, and other metals have become the first option for microjetting study. The metal studied in this paper is tin, which is a very widely used material in experiment. Tin is an interesting metal because it has a stable room tem-

perature solid phase (β_{phase}) of body-centered tetragon (BCT). When tin is impacted, it will form a denser BCT phase. If the impact is strong enough, it can also go directly into the liquid phase. When $P_{\text{SB}} \geq 19.5$ GPa, the gamma phase will unload and melt. When 33 GPa $\geq P_{\text{SB}} \geq 19.5$ GPa, it will be in the solid-liquid coexisting phase under unloading. The high strain rate of shock loading is likely to result in the unloading and melting of the metal, in order to more easily and more in depth explore the factors that affect the results of the microjetting, monocrystalline tin and polycrystalline tin are obviously a reliable option.

2.2. Model description

The initial structure of the monocrystalline tin and polycrystalline tin models are shown in Fig. 1. For the convenience of description, we denote "I" as monocrystalline tin sample composed of 1 crystal grain, and "II" and "III" as polycrystalline tin samples composed of 36 crystal grains and 144 crystal grains, respectively. Hereafter we will directly use I, II, and III to represent the three tin samples unless otherwise stated. There is a sinusoidal defect at the right end of the model where the amplitude is $h_0 = 7$ nm (the distance from the top of the defect to the valley bottom is $2h_0 = 14$ nm), and the wavelength $\lambda = 50$ nm. The model structure is the BCC crystal structure, in which the lattice constant is 3.7 Å. The x, y, and z axes are along the [100], [010], and [001] crystal directions, respectively. The sizes in three-dimensional directions are $L_x = 389.5$ nm, $L_y = 50.0$ nm, and $L_z = 5.3$ nm for each of monocrystalline tin and polycrystalline tin. Since the size of monocrystalline tin model and polycrystalline tin model are the same, they both contain about 4 million atoms. In order to obtain stable structure at room temperature, the initial structure of monocrystalline tin and polycrystalline tin are first heated in the system to 300 K for a period of relaxation, and then cooled it to 10 K for a period of relaxation. The process is carried out under zero pressure in constant temperature isobaric ensemble under three-dimensional periodic boundary condition. The calculated time step is 1 fs and the impact loading of the plate is obtained by the piston method, where a 3-nm unforced block is fixed as a rigid piston, and an initial velocity in the x direction is used.

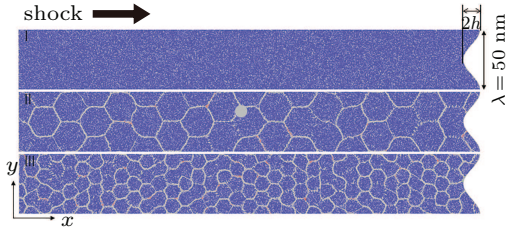


Fig. 1. Initial model of monocrystalline tin and polycrystalline tin. where "I" represents monocrystalline tin composed of 1 crystal grain, "II" and "III" denote polycrystalline tins composed of 36 crystal grains and 144 crystal grains, respectively.

3. Results and discussion

3.1. Comparison of jet head velocity between monocrystalline tin and polycrystalline tin

Solid lines, triangles and circles of Fig. 2(a) represent I, II, and III, respectively, showing the evolution of the jet head velocity with time under four different impact velocities. Figure 2(b) shows the changes of jet head velocity of three tin samples with pressure of near free surface. According to Fig. 2(a), it is not difficult to find that the changing trends of the jet head velocity of three tin samples are consistent under different impact loading intensities. When the shock wave reaches the bottom of the defect, the jet head velocities of three tin samples increase significantly. However, it can be found that the jet head velocity presents a plateau at about 8 ps, when impact strength is 0.6 km/s. This is because when the impact velocity is low, the jet head velocity increases relatively slowly. As shown in Fig. 2(a), the time for the jet head velocity of monocrystalline tin and polycrystalline tin to reach their peaks is almost the same under the same impact strength. When impact strength is 0.6 km/s, 0.9 km/s, 1.2 km/s, and 1.5 km/s, the corresponding time to reach peak of jet head velocity is 7.5 ps, 8.5 ps, 9.0 ps, 12.5 ps, respectively. What should be pointed out is that different impact pressures need different times to reach the peak of the jet head velocity, whether it is monocrystalline tin or polycrystalline tin. This result also indicates that the time for the jet head velocity to reach the peak decreases with the increase of impact intensity, and when the jet head velocity reaches the peak, there appears the attenuation to a certain extent. varying degrees of attenuation. Specifically, when the impact strength is 0.6 km/s, 0.9 km/s, 1.2 km/s, and 1.5 km/s, the corresponding attenuation is 0.39, 0.30, 0.16, and 0.15, respectively. It can be clearly seen that when impact strength is 1.2 km/s and 1.5 km/s, the drop range of jet head velocity is relatively limited. However, when the impact strength is 0.6 km/s and 0.9 km/s, the jet head velocity drops significantly, which is due to the surface tension effect. In fact, previous studies also claim that surface tension on a nanometer scale can significantly reduce the jet head velocity under the low impact strength.[16,34] In addition, Wu *et al*. further explained that the partial kinetic energy is converted into surface energy in the jetting process, but partial kinetic energy is converted into surface energy which accounts for a small fraction under the high impact strength. Especially under the low impact strength, surface energy can hinder the jetting.[35] Therefore, this effect that cannot be neglected results in a significant decrease of the jet head velocity. Figure 2(b) shows the relation between jet head velocity and near free surface pressure. Here, we make a comparison of microjetting between monocrystalline tin and polycrystalline tin under plane impact loading. When the impact pressure is low, the jet head velocity of monocrystalline

tin is higher than polycrystalline tin's, but after the impact strength increases, the two jet head velocities are almost the same as the impact pressure increases.

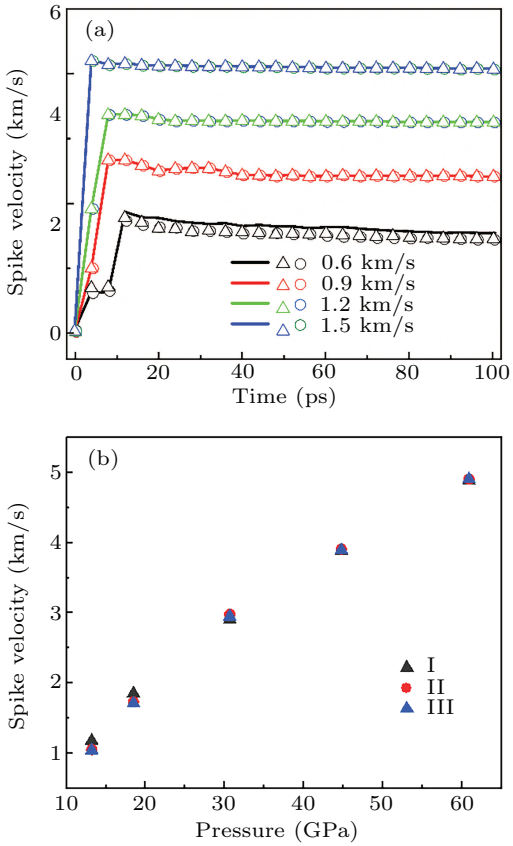


Fig. 2. (a) Evolutions of jet head velocity with time under four different impact velocities and (b) variations of jet head velocity with pressure near free surface, for I (solid line), II (triangle), III (circles).

In order to discuss the above phenomena, we use the method of analyzing the shock wave profile, particle tracking and crystal structure. The above MD simulation studies have shown that the jet head velocity depends mainly on the instantaneous impact pressure close to the defect surface. Even if the impact shape varies greatly due to the difference in loading method, the resulting jet head velocities will be consistent as long as the impact pressures reaching at the defect are the same.[35,36] Therefore, it needs to take only two different impact pressures to compare the impact pressure profiles approaching to the near free surface. As shown in Fig. 3(a), it can be clearly seen that the shock wave of shock loading polycrystalline tin begins to attenuate at 350 nm, and the shock wave pressure of shock loading monocrystalline tin near the free surface is significantly stronger than that of polycrystalline tin. The previous MD researches indicate that the shock wave attenuation phenomenon is mainly due to the anisotropy of the grains in the polycrystalline and the grain boundary scattering, but this effect will gradually decrease as the impact strength increases. Later, deduced from the experimental results of coarse-grained materials is also a consistent understanding.[37] Owing to the attenuation of the front-end shock wave, the jet head velocity is related only to the shock wave intensity close to the defect surface. In Fig. 3(b), the shock wave pressure of the shock loading polycrystalline tin is almost consistent with that of the shock loading monocrystalline tin, and there is no obvious attenuation in the two pressures. It is not difficult to explain why the jet head velocity of polycrystalline tin is lower than that of monocrystalline tin at low impact velocity. With the increase of impact velocity, the velocities of the shock waves near the free surface are similar, so that the jet head velocity of monocrystalline tin is consistent with that of polycrystalline tin.

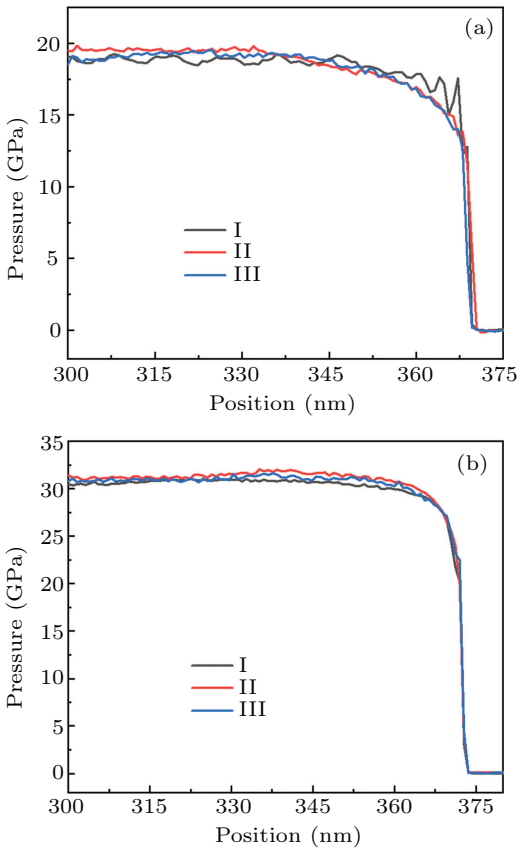


Fig. 3. Impact pressure profile under impact velocities of (a) 0.6 km/s and (b) 0.9 km/s for I, II, and III.

3.2. Comparison of jet morphology between monocrystalline tin and polycrystalline tin

Figure 4(a) shows the atomic diagram of initial structure of monocrystalline tin and polycrystalline tin composed of 36 grains at 70 ps, which is obtained by the particle tracking method. Since the jet head velocity of the polycrystalline tin composed of 36 grains and that of polycrystalline tin composed of 144 grains are the same when the shock velocity is 0.6 km/s, we need to pay attention only to the difference between the microjetting results of monocrystalline tin and polycrystalline tin composed of 36 grains. For the convenience of description, the polycrystalline tin mentioned later in this section is composed of 36 grains. Figures 4(c) and 4(d) are the source positions of the jet in Figs. 4(a) and 4(b) in

the initial structure, respectively. Figures 4(a) and 4(c) show the atomic diagram of initial structure of monocrystalline tin, and figures 4(b) and 4(d) display the atomic diagram of initial structure of polycrystalline tin. The color division of Fig. 4(a) is to take 10 nm downward from the top of the jet as the red part, the range below the red part and above the free surface as the green part, and the range below the green part and above the block part is taken as the blue part. The red part and the green part are above the free surface, and their sum is regarded as the jet mass. It can be seen from Fig. 4(a) that the jet formed by the defect part is stratified, and the red part closest to the defect is ejected first, followed by the green part, and finally the blue part. But it should be noted that the atoms of red part and green part are close mainly to the defect, while the atoms of blue part are more on both sides. This is because the atoms on both sides are close to the surface, which distribution is similar to the scenario of the free surface. The aforementioned results about plane impact loading monocrystalline tin and polycrystalline tin are almost the same. As shown in Figs. 4(c) and 4(d), the injection source part of the polycrystalline tin is not so uniformly symmetrical as that of the monocrystalline tin along the central axis of the defect, and the number of its blue atoms formed on both sides of polycrystalline tin is obviously more than that of the monocrystalline tin. In addition, under an impact loading of 0.6 km/s, we also find that not only the jet velocity of polycrystalline tin is lower than that of monocrystalline tin, but also the jet formed by polycrystalline tin is not symmetrical along the central axis. In fact, when the shock wave reaches the bottom of the defect, it will have a complex interaction with the grain boundaries. Hence, we infer that the existence of different grain boundaries and grain orientations is one of important reasons for the phenomenon. Li *et al*.'s

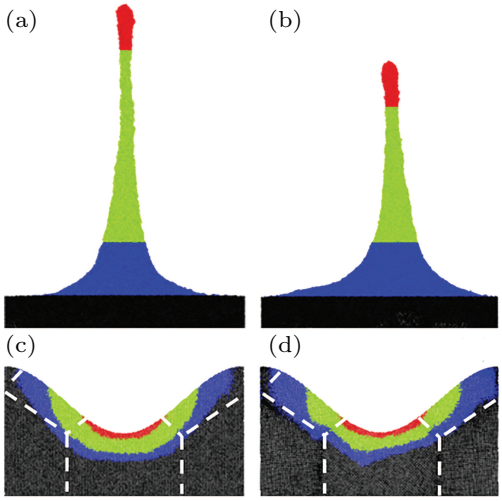


Fig. 4. Comparison of jet and jet source between monocrystalline tin and polycrystalline tin, with the same color representing the same atom, and white dotted line denoting the position of polycrystalline grain boundary: (a) jet of monocrystalline tin at 70 ps and impact velocity 0.6 km/s; (b) jet of polycrystalline tin at 70 ps and impact velocity 0.6 km/s; (c) jet source position of monocrystalline tin at 0 ps and impact velocity 0.6 km/s; (d) jet source position of polycrystalline tin at 0 ps and impact velocity of 0.6 km/s.

study deems that the atoms near the defect absorb energy to eject along the symmetrical direction of the central axis after the shock wave reaches the defect.[36] Therefore, obviously, the atoms on the left side of the center axis in Fig. 4(d) absorb more energy, and the jet is ejected along the right side of the center axis, which is the main reason for the jet deflection.

In order to further explore the influence of the crystal structure on the jet, we specially compare the jets at impact velocities of 0.45 km/s, 0.6 km/s, 0.9 km/s, 1.2 km/s, 1.5 km/s and analyze the crystal structure by ACNA analysis method, and the results are shown in Fig. 5. The results show that the jet of monocrystalline tin is always on the central axis, while the jet head of polycrystalline tin deviates from the central axis when the impact velocity is 0.45 km/s and 0.6 km/s. For polycrystalline tin, the deviation scale corresponding to the impact velocity of 0.6 km/s is less than that of 0.45 km/s as indicated in Figs. 5(b) and 5(d). Figures 5(f)–5(h), show that when the impact velocity is 0.9 km/s, only the middle part deviates from the central axis, the front end of the jet is still on the central axis. But when the impact velocity is 1.2 km/s and 1.5 km/s, jets are on the central axis. According to Fig. 5 obtained by crystal structural analysis, it can be seen that the deviated direction of the jet is close to the parts with more main crystal structure. This is because the melting area is beneficial to the jetting process, and this non-uniform melting causes the jet to be deflected. The atoms in the molten parts possess liquid fluidity, so they are easier to break through the strength of the material and eject. For the polycrystalline tin under the impact velocity of 0.9 km/s, the ACNA analysis[38] shows that the crystal melting degree increases as the impact pressure increases, and the surface that melts first is the main part that forms the front of the jet. When the impact velocity is 0.9 km/s, the main part of the polycrystalline tin still has a crystal structure, which results in the front end of the jet still on the central axis and the middle end deviates from the central axis. Therefore, we can draw a conclusion that comparing with the middle end of the jet, the pressure required for the front end of the jet to be symmetrical with respect to the central axis is small on a nanometer scale. Moreover, the jet produced by the polycrystalline tin at the impact velocity of 1.2 km/s and that at the impact velocity of 1.5 km/s have almost no deflection, which further indicates that the jet deviation is caused mainly by the non-uniform melting of the loaded sample with the different grain orientations and grain boundaries. As a result, once the surface is melted completely, the jet will no longer deviate. When the shock wave velocity increases, the jet is easier to eject symmetrically along the central axis. The comparative results of microjetting generated by monocrystalline tin and polycrystalline tin under plane impact loading show that the non-uniform melting of the sample also has a significant effect on the jet direction. Furthermore, we suspect that the compli-

cated scattering effect of grain boundaries and the different grain orientations are physical mechanism that is responsible for this phenomenon.

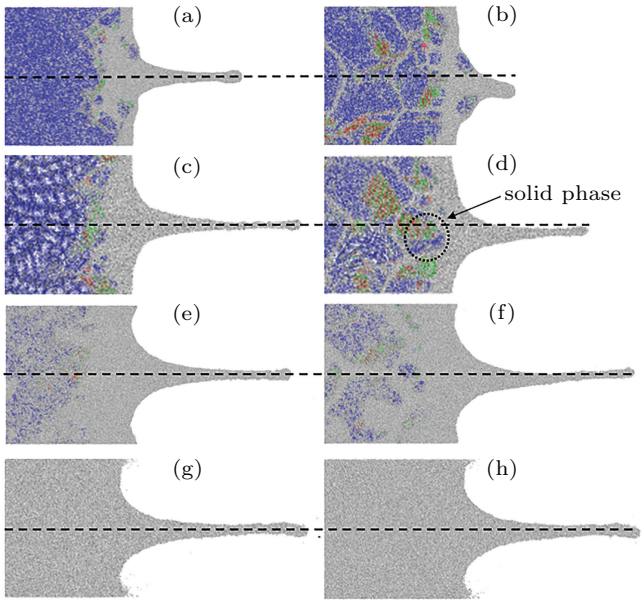


Fig. 5. Jets of monocrystalline tin and polycrystalline tin at different impact velocities, obtained from ACNA analysis, with black dotted line referring to symmetrical auxiliary line: (a) jet of monocrystalline tin at 100 ps and impacted velocity 0.45 km/s; (b) jet of polycrystalline tin at 100 ps and impacted velocity 0.45 km/s; (c) jet of monocrystalline tin at 70 ps and impacted velocity 0.6 km/s; (d) jet of polycrystalline tin at 70 ps and impacted velocity 0.6 km/s; (e) jet of monocrystalline tin at 50 ps and impacted velocity 0.9 km/s; (f) jet of polycrystalline tin at 50 ps and impacted velocity of 0.9 km/s; (g) jet of polycrystalline tin at 42 ps and impacted velocity 1.2 km/s; (h) jet of polycrystalline tin at 39 ps and impacted velocity of 1.5 km/s.

3.3. Comparison of jet mass coefficient and jet velocity coefficient between monocrystalline tin and polycrystalline tin

Figure 6 shows the calculated curves of the jet velocity coefficient *versus* impact velocity, and curves of jet mass coefficient *versus* impact velocity of monocrystalline tin and polycrystalline tin. The jet mass of many materials was deemed to be exactly equal to the mass of the prefabricated defects in the initial structure according to a lot of experiments, so the jet mass coefficient has been widely used in the microjetting experiment research.[8,10,39] The jet mass coefficient is defined as the ratio of jet mass to defect mass, namely,

$$R_{\mathrm{m}} = \frac{M_j}{M_{\mathrm{def}}}, \tag{5}$$

where M_j is the jet mass of the part beyond the free surface, and M_{def} is the defect mass in the initial configuration. The jet velocity coefficient is defined as the ratio of the jet head velocity to the free surface velocity, namely,[39]

$$R_{\mathrm{u}} = \frac{u_j^{\max}}{u_{\mathrm{fs}}}, \tag{6}$$

where $u_j^{\max}$ is the jet head velocity, and u_{fs} is the free surface velocity.

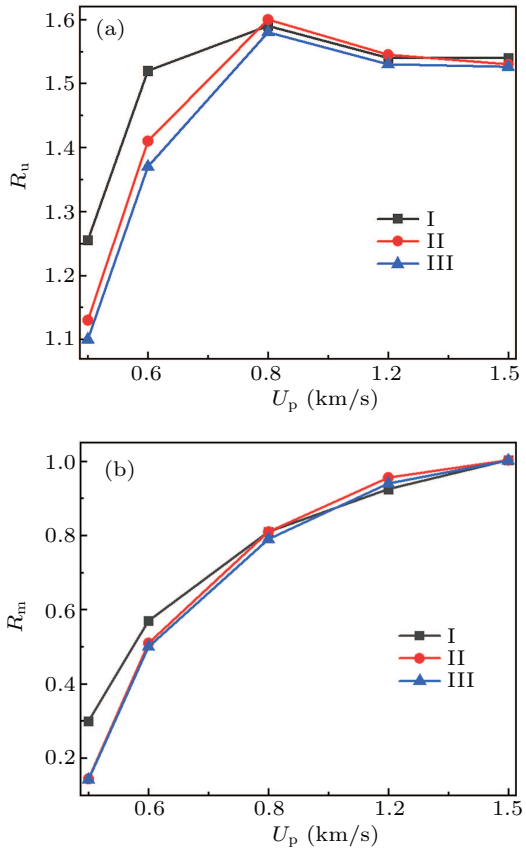


Fig. 6. (a) Curves of jet velocity coefficient *versus* impact velocity and (b) curves of jet mass coefficient *versus* impact velocity for I, II, and III.

As shown in Fig. 6(a), the jet velocity coefficient of monocrystalline tin at low impact velocity is significantly larger than that of polycrystalline tin (whether it is composed of 36 grains or 144 grains). It is mainly due to the influence of the grain orientations and grain boundary scattering of polycrystalline tin at low impact velocity on the jet head velocity, which results in a decrease in the jet velocity coefficient of the polycrystalline tin at low impact velocity. As shown in Fig. 6(b), it is not difficult to find that the jet mass coefficient increases and tends to be stable with the increase of the impact velocity. The jet mass coefficient of monocrystalline tin is significantly larger than that of polycrystalline tin under the impact velocity of 0.45 km/s, but with the increase of the impact velocity, the gap of the jet mass coefficient gradually narrows. When the impact velocity is beyond 0.9 km/s, the value of the jet mass coefficient begins to tend to be the same. According to formula (5), whether monocrystalline tin or polycrystalline tin, as long as the mass of the prefabricated defects of the monocrystalline tin is the same as that of the polycrystalline tin, finally their jet mass coefficients will trend to be the same with the increase of impact velocity, specifically, the two values will be close to 1. This is because the influence of grain orientation and grain boundary scattering effect can be ignored under high-intensity impact, and almost all of the prefabricated defects can be ejected. The above results also illustrate from the side that the influence of grain boundary

scattering effect and grain orientations at low impact cannot be ignored.

4. Conclusions

This paper mainly uses the MD simulation method of the EAM interaction potential to study the microjetting phenomenon in the monocrystalline tin and polycrystalline tin under the plane impact loading, with initial sinusoidal defects of tin sample taken into consideration. The features of microjetting in monocrystalline tin and polycrystalline under plane impact loading are investigated from aspects of jet head velocity, jet morphology, jet mass coefficient, and jet velocity coefficient. Comparing with monocrystalline tin, defects such as the grain orientation and grain boundaries of the polycrystalline tin under low velocity more easily cause the polycrystalline surface to melt non-uniformly and the shock wave front to attenuate. The non-uniform melting leads the jet to deviate, but the surface of polycrystalline tin melts completely and the jet no longer deviates when the impact velocity reaches 1.2 km/s. The jet head velocity, jet velocity coefficient and jet mass coefficient of polycrystalline tin at low impact velocity are all lower than those of monocrystalline tin, but these results of the two samples are almost the same when the impact velocity is greater than or equal to 0.9 km/s. The research results in this article can provide some help to explain the microjetting mechanism of polycrystalline tin, and provide corresponding guidance for the research and development of weapon engineering. The present research in this article is relatively simple, and surely there exist certain shortcomings. In the future, we will focus on particle fragmentation, gas–solid–liquid coupling, *etc*. in the microjetting process, thereby presenting more effective information for the research of microjetting.

References

[1] Amouye F A and Niknam A R 2018 *J. Appl. Phys.* **123** 043106
[2] Liu Y and Grieves B 2014 *J. Fluids Eng.* **136** 091202
[3] Durand O and Soulard L 2015 *J. Appl. Phys.* **117** 165903
[4] Monfared S K, Oro D M, Graver M, Hammerberg J E, Lalone B M, Pack C L, Schauer M M, Stevens G D, Stone J B and Turley W D 2014 *J. Appl. Phys.* **116** 063504
[5] Buttler W T, Oró D M, Preston D L, Mikaelian K O, Cherne F J, Hixson R S, Mariam F G, Morris C, Stone J B and Terrones G 2012 *J. Fluid Mech.* **703** 60
[6] Dimonte G and Ramaprabhu P 2010 *Phys. Fluids* **22** 014104
[7] Dimonte G, Terrones G, Cherne F J and Ramaprabhu P 2013 *J. Appl. Phys.* **113** 024905
[8] Zellner M B, Grover M, Hammerberg J E, Hixson R S, Iverson A J, Macrum G S, Morley K B, Obst A W, Olson R T and Payton J R 2007 *J. Appl. Phys.* **102** 013522
[9] Zellner M B, Mcneil W V, Hammerberg J E, Hixson R S, Obst A W, Olson R T, Payton J R, Rigg P A, Routley N and Stevens G D 2008 *J. Appl. Phys.* **103** 113508
[10] Ren G W, Zhang S W, Hong R K, Tang T G and Chen Y T 2016 *Chin. Phys. B* **25** 086202
[11] De Rességuier T, Lescoute E, Sollier A, Prudhomme G and Mercier P 2014 *J. Appl. Phys.* **115** 043525
[12] Chu G B, Xi T, Yu M H, Fan W, Zhao Y Q, Shui M, He W H, Zhang T K, Zhang B, Wu Y C, Zhou W M, Cao L F, Xin J T and Gu Y Q 2018 *Rev. Sci. Instrum.* **89** 115106
[13] Vogan W S, Anderson W W, Grover M, Hammerberg J E, King N S P, Lamoreaux S K, Macrum G, Morley K B, Rigg P A and Stevens G D 2005 *J. Appl. Phys.* **98** 113508
[14] Holtkamp D B, Clark D A, Ferm E N, Gallegos R A, Hammon D, Hemsing W F, Hogan G E, Holmes V H, King N S P, Liljestrand R, Lopez R P, Merrill F E, Morris C L, Morley K B, Murray M M, Pazuchanics P D, Prestridge K P, Quintana J P, Saunders A, Schafer T, Shinas M A and Stacy H L 2004 *AIP Conf. Proc.* **706** 477
[15] Roland C, de Rességuier T, Sollier A, Lescoute E, Soulard L and Loison D 2017 *AIP Conf. Proc.* **1793** 100027
[16] Dyachkov S, Parshikov A and Zhakhovsky V 2017 *AIP Conf. Proc.* **1793** 100024
[17] Soulard L 2008 *Eur. Phys. J. D* **50** 241
[18] Durand O and Soulard L 2017 *J. Dynamic Behavior Mater.* **3** 280
[19] Durand O, Soulard L, Bourasseau E and Filippini G 2016 *J. Appl. Phys.* **120** 045306
[20] Meyers M A 1977 *Mater. Sci. Eng.* **30** 99
[21] Barber J L 2008 *Phys. Rev. B* **77** 144106
[22] Kadau K, Germann T C, Lomdahl P S, Albers R C, Wark J S, Higginbotham A and Holian B L 2007 *Phys. Rev. Lett.* **98** 135701
[23] Alder B J and Wainwright T E 1957 *J. Chem. Phys.* **27** 1208
[24] Leimkuhler B and Matthews C 2016 *Proc. Roy. Soc. A: Math. Phys. Eng. Sic.* **472** 20160138
[25] Hansson T, Oostenbrink C and van Gunsteren W 2002 *Curr. Opin. Struct. Biol.* **12** 190
[26] Xiong Q L, Kitamura T and Li Z H 2019 *J. Appl. Phys.* **125** 194302
[27] Rapaport D C 1999 *Mol. Dyn. Simul. Comput. Sci. Eng.* **1** 70
[28] Plimpton S 1995 *J. Comput. Phys.* **117** 1
[29] Vella J R, Chen M, Stillinger F H, Carter E A and Debenedetti P G 2017 *Phys. Rev. B* **95** 064202
[30] Etesami S A, Baskes M I, Laradji M and Asadi E 2018 *Acta Mater.* **161** 320
[31] Ko W S, Kim D H, Kwon Y J and Lee M H 2018 *Metals* **8** 900
[32] Sapozhnikov F A, Ionov G V, Dremov V V, Soulard L and Durand O 2014 *J. Phys. Conf. Ser.* **500** 032017
[33] Daw M S and Baskes M I 1983 *Phys. Rev. Lett.* **50** 1285
[34] Durand O, Jaouen S, Soulard L, Heuzé O and Colombet L 2017 *J. Appl. Phys.* **122** 135107
[35] Wu B, Wu F C, Zhu Y B, Wang P, He A M and Wu H A 2018 *AIP Adv.* **8** 045002
[36] Li B, Zhao F P, Wu H A and Luo S N 2014 *J. Appl. Phys.* **115** 349
[37] Chhabildas L C and Asay J R 1979 *J. Appl. Phys.* **50** 2749
[38] Stukowski A, Bulatov V V and Arsenlis A 2012 *Model. Simul. Mater. Sci. Eng.* **20** 085007
[39] Asay J R, Mix L P and Perry F C 1976 *Appl. Phys. Lett.* **29** 284